RSC Advances

PAPER

View Article Online
View Journal | View Issue

Cite this: *RSC Adv.*, 2017, **7**, 35257

Influence of precursor pH on the structure and photo-Fenton performance of Fe/hydrochar

Chuan Liang, Wei Zhao, Zhuda Song and Shengtao Xing *

Fe/hydrochar was one-pot synthesized by a hydrothermal method under different pH conditions. The structure, composition and chemical state of the obtained samples were analyzed by different characterization methods. It was found that the precursor pH affected the morphology, surface area, surface Fe content and organic groups of the products. The catalytic performance of the samples for the photo-Fenton decolorization of Orange II with visible light irradiation and the role of dissolved Fe in this process were investigated. The result indicated that the Fe/hydrochar prepared at pH 2 exhibited the highest catalytic activity because of its strong visible light adsorption, high surface Fe content, and rich oxygen-containing groups. The light irradiation accelerated the leaching of Fe and regeneration of Fe^{2+}, and the contribution of homogeneous reactions increased dramatically with reaction time, thus promoting the formation of $^{\bullet}OH$ in solution. A possible mechanism for the Fe^{3+}/Fe^{2+} cycle at the catalyst/water interface was proposed.

Received 3rd June 2017
Accepted 8th July 2017

DOI: 10.1039/c7ra06194c

rsc.li/rsc-advances

Introduction

Water pollution with toxic organic pollutants has been attracting considerable attention because of its detrimental effects on the environment and human health. The heterogeneous Fenton process is well considered as an efficient technology for water treatment since it can generate highly reactive radicals, such as hydroxyl radicals ($^{\bullet}OH$), for complete oxidation of refractory organic pollutants.[1,2] Up to now, many Fe-based solid catalysts have been synthesized and their catalytic mechanisms have also been studied.[3–9] It was found that the recovery of Fe^{2+} from Fe^{3+} is extremely slow, and the sustained production of $^{\bullet}OH$ is very limited. Thus, a heterogeneous Fenton system is frequently combined with ultraviolet (UV) light, ultrasonic or electrochemical technology to promote the production of active radicals.[10–12] However, these methods would significantly increase the treatment cost.

Recently, visible light photo-Fenton process has become a hot research topic because of its low cost and easy operation, and the preparation of efficient catalysts has received more attention. Some researchers found that the supported and unsupported Fe exhibited good photo-Fenton activity for the decolorization of organic dyes at pH $\leq$ 4, and in which dye photosensitization played a key role.[13–17] The excited dye molecules with visible light irradiation can reduce Fe^{3+} to Fe^{2+}, thus promoting the formation of $^{\bullet}OH$. Various iron containing semiconductor catalysts have also been applied in photo-Fenton reactions.[18–23] The catalysts can generate electrons and holes under visible light irradiation, and the photogenerated electrons can effectively promote the regeneration of Fe^{2+}. In addition, H_2O_2 might possibly react with the photogenerated electrons to produce $^{\bullet}OH$. To accelerate the separation of photogenerated charge carriers, carbonaceous materials such as graphene and carbon nanotube were introduced into the photo-Fenton catalyst, and a positive effect was obtained.[24–27] More recently, hydrochar (HC) prepared *via* the hydrothermal treatment of biomass has been widely used as cost-effective and green water purification materials.[28–32] With the introduction of metal salts into this hydrothermal process, carbon-encapsulated core–shell composites and hybrids could be obtained. It was found that metal ions and metal oxide nanoparticles could accelerate the hydrothermal carbonization process, and the obtained metal or metal oxide/HC composites exhibited excellent activity for the removal of organic pollutants in water. For instance, Luo *et al.* reported that magnetite/carboxylate-rich HC exhibited excellent photodegradation activity at neutral pH under visible light irradiation.[33] Sun *et al.* found that nano zero-valent iron encapsulated in HC showed an efficient Fenton-like activity for the degradation of phenol.[34,35] The performance of the HC catalysts is tightly associated with their structure and composition, which are dependent on the preparation method. Although the synthesis of Fe/HC has been reported by several groups, the influence of precursor pH, a key parameter in hydrothermal process, on its structure and visible light photo-Fenton activity has been rarely studied.

Herein, Fe/hydrochar (Fe/HC) was prepared by a hydrothermal method and investigated as a visible light photo-Fenton catalyst. The influences of precursor pH on the

College of Chemistry and Material Sciences, Hebei Normal University, Shijiazhuang, 050024, PR China . E-mail: stxing07@sina.com; Fax: +86 311 80787402; Tel: +86 311 80787400

structure, composition and chemical state of the catalyst were analyzed by different characterization methods, and their correlation with photo-Fenton activity was also investigated. The roles of hydrochar, active radicals and homogeneous Fenton reaction in this photo-Fenton process were discussed, and a possible catalytic mechanism was proposed.

Experimental

Catalyst preparation

All the chemicals were of analytical grade and used as received without further purification. Fe/HC was prepared by a hydrothermal method. Firstly, $Fe(NO_3)_3$ and glucose with the mole ratio of 1 : 6 were dissolved in deionized water under stirring. The solution was adjusted to a certain pH by addition of HNO_3 or NaOH solution and magnetically stirred for 1 h. The mixture was transferred into a 100 mL Teflon-lined stainless steel autoclave tube and heated in an oven at 180 °C for 12 h. The obtained solid product was washed with NaOH solution to remove adsorbed organic acids, then washed with deionized water until the filtrate was neutral, and finally dried at 60 °C for 12 h. The samples prepared at pH 2, 4, 6 and 8 were designated as Fe/HC-2, Fe/HC-4, Fe/HC-6 and Fe/HC-8.

Catalyst characterization

Powder X-ray diffraction (XRD) analysis was performed on a Bruker D8-Advance diffractometer using Cu Kα radiation. The morphologies of the samples were examined by a Hitachi S-4800 field emission scanning electron microscopy (FESEM). Nitrogen adsorption–desorption isotherms were obtained at −196 °C using a Quantachrome NOVA 4000e surface area analyzer. Infrared (IR) spectra were recorded on a Nicolet iS 50 Fourier transformation infrared spectrometer. X-ray photoelectron spectroscopy (XPS) analysis was performed on a Shimadzu ESCA-3400 spectrometer (Mg Kα radiation). The zeta potential of the catalyst suspension at different pH was determined by a Malvern 3000 Zetasizer.

Catalytic activity measurements

Catalytic degradation of Orange II aqueous solution (10 mg L^{-1}) was conducted in a 200 mL cylindrical glass vessel with a circulating water jacket for cooling. A 300 W Xe lamp (PLS-SXE300c, Perfectlight) with a UV cutoff filter ($\lambda \geq 420$ nm) was placed upside the vessel. In a typical experiment, 0.05 g of catalyst was dispersed in 100 mL of Orange II aqueous solution and magnetically stirred in dark for 30 min to achieve adsorption/desorption equilibrium. The solution pH was adjusted by dilute H_2SO_4 and NaOH aqueous solutions. Subsequently, a certain amount of H_2O_2 (10 mM) was added and the lamp was turned on immediately. At given time intervals, samples were filtered through a Millipore filter (pore size 0.25 μm) for analysis. The concentration of Orange II was measured using a UV-vis spectroscope (UV-7504) at 485 nm. The concentrations of Fe^{2+} and total Fe in solution were determined using a phenanthroline spectrophotometric method and an atomic absorption spectrometer (180-70, Hitachi, Japan), respectively.[36] The formation of ˙OH was determined by a fluorescence method using *p*-phthalic acid (PTA) as the probe because PTA can react with ˙OH to form a product (2-hydroxyl *p*-phthalic acid) with fluorescence at 455 nm. The reaction product was measured with a Hitachi F-4600 fluorescence spectrometer excited at 332 nm. The results are the averages of duplicate or triplicate experiments.

Results and discussion

Characterization of Fe/HC

The XRD patterns of the prepared samples are shown in Fig. 1. A broad peak in the 2θ range of 10–30° can be observed for all samples, which can be assigned to amorphous and non-graphitic carbon.[37,38] Apart from the diffraction of carbon, a weak peak at 35.4° can be observed for Fe/HC-4 and Fe/HC-6, which can be ascribed to FeOOH or Fe_2O_3.[32] No other diffraction peaks of iron oxides were observed, indicating that the loaded Fe was amorphous. The SEM images in Fig. 2 show that carbon microspheres can be obtained under different pH. The sizes of these spheres were much larger than that of carbon nanospheres obtained in the absence of iron precursor, which is in accordance with the literature.[34] In addition, some irregular particles were also produced for all samples. The microspheres obtained at pH 4 were more smooth and uniform, and the content of irregular particles was much lower. Some large aggregated particles were produced at pH 6 and the sizes of the aggregates decreased significantly with increasing pH to 8.

Fig. 3 shows the N_2 adsorption–desorption isotherms of the samples. All the isotherms are type IV with a hysteresis loop, indicating the presence of mesopores. The steep increasing at relative high pressures ($0.8 < P/P_0 < 0.95$) could be attributed to the large pores formed between particles. The surface areas of Fe/HC-2, Fe/HC-4, Fe/HC-6 and Fe/HC-8 were calculated to be about 11.7, 34.1, 18.1 and 31.3 $m^2\ g^{-1}$, respectively. All the samples showed a narrow pore size distribution centered at 3–4 nm. The pore volumes of Fe/HC-2, Fe/HC-4, Fe/HC-6 and Fe/HC-8 were 0.061, 0.163, 0.104 and 0.155 $cm^3\ g^{-1}$, respectively.

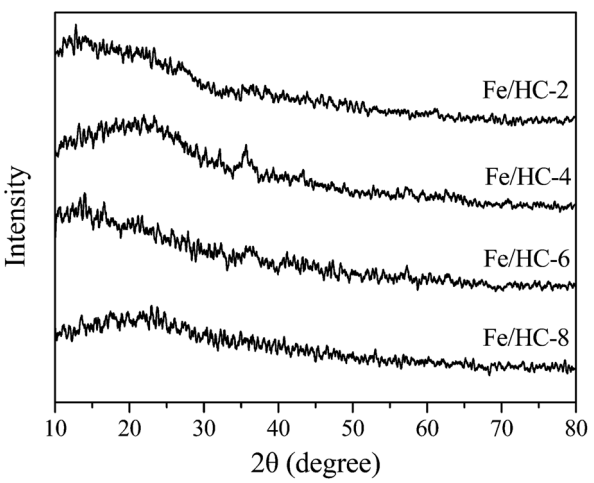

Fig. 1 XRD patterns of different Fe/HC samples.

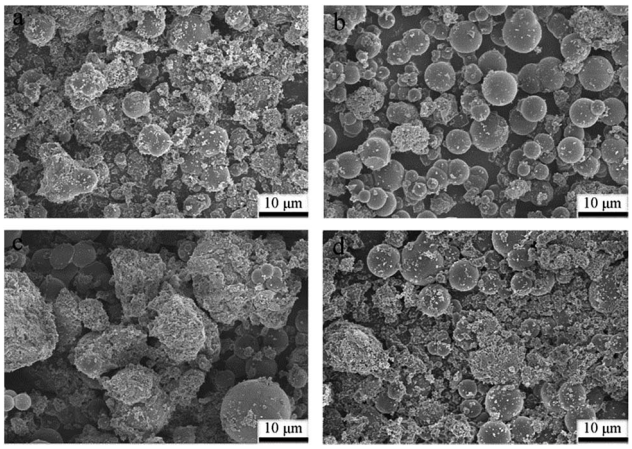

Fig. 2 SEM images of (a) Fe/HC-2, (b) Fe/HC-4, (c) Fe/HC-6 and (d) Fe/HC-8.

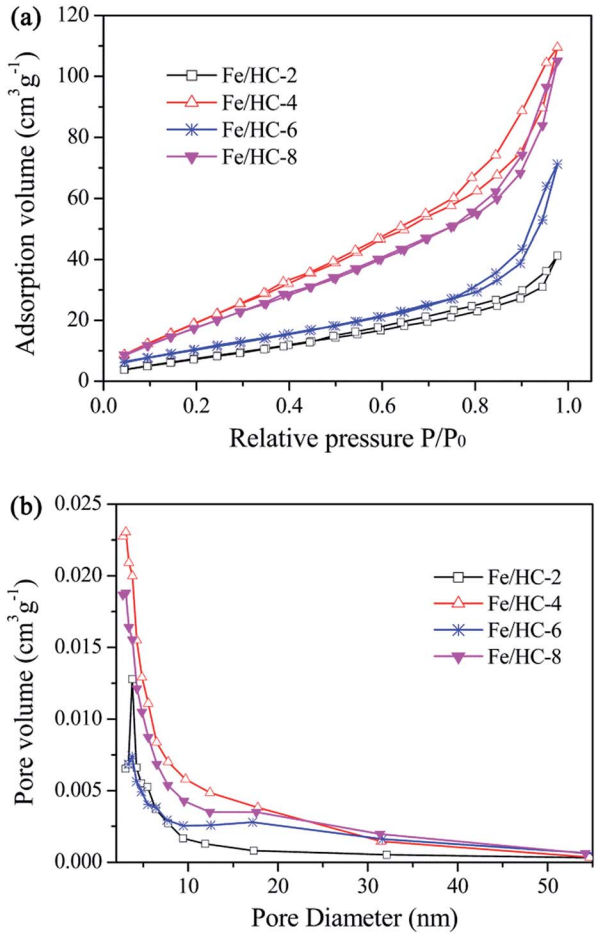

Fig. 3 Nitrogen adsorption–desorption isotherms (a) and pore sized distribution (b) of different Fe/HC samples.

The FTIR spectra of the samples are shown in Fig. 4. All the samples exhibited similar spectra, and some carbon-containing functional groups can be observed.[39–41] The broad band at 3430 cm^{-1} can be assigned to the stretching vibration of O–H

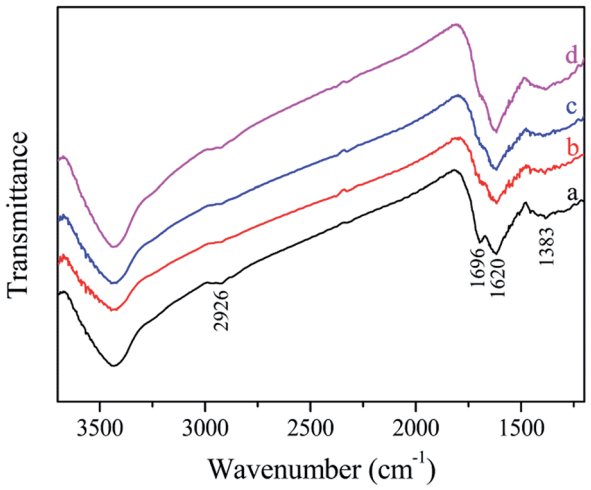

Fig. 4 FTIR spectra of different Fe/HC samples: (a) Fe/HC-2, (b) Fe/HC-4, (c) Fe/HC-6 and (d) Fe/HC-8.

(hydroxyl or carboxyl). The bands at 2926 cm^{-1} can be ascribed to the stretching vibration of C–H. The bands at 1696 and 1618 cm^{-1} can be attributed to C=O and C=C vibrations, respectively, which reveal the oxidation, dehydration and aromatization of glucose during the hydrothermal treatment. The weak peak at 1383 cm^{-1} may be due to the adsorbed nitrate.

The surface composition and metal oxidation state of Fe/HC were further investigated by XPS. The surface content of Fe was measured to be 2.87, 2.47, 2.43, and 1.86 at% for Fe/HC-2, Fe/HC-4, Fe/HC-6 and Fe/HC-8, respectively. N was also observed on the surface, demonstrating the presence of nitrate. In order to determine the bulk content of Fe, the sample was heated at 500 °C for 4 h in air, then dissolved by HCl solution. The Fe concentration in the solution was measured by an atomic absorption spectrometer. It was found that the bulk Fe content of Fe/HC-2 (4.33 wt%) was much lower than that of the other three samples (5.48–5.53 wt%), which was opposite to their surface content. Since iron ions were precipitated at higher pH and the precipitate could be encapsulated by hydrochar during the hydrothermal treatment, the surface Fe content of Fe/HC decreased with increasing precursor pH. Fig. 5 shows the XPS Fe 2p and C 1s spectra. The peaks at about 711, 718 and 724 eV can be attributed to Fe $2p_{3/2}$, shake-up satellite Fe $2p_{3/2}$, and Fe $2p_{1/2}$, respectively. The Fe $2p_{3/2}$ peak can be deconvoluted into two peaks with binding energies at 710.3–710.7 and 713.2–713.9 eV, indicating the simultaneous presence of Fe^{2+} and Fe^{3+} species.[42] The Fe^{2+}/Fe^{3+} ratio was calculated to be 2.41, 2.11, 2.17 and 2.09 for Fe/HC-2, Fe/HC-4, Fe/HC-6 and Fe/HC-8, respectively. The result indicated that Fe^{2+} ions were the main Fe species. The C 1s spectra of the samples were deconvoluted into four component peaks, which could be attributed to R–C_6H_5, C–O, C=O and O–C=O, respectively.[40,43] The contents of oxygen-containing groups (C–O, C=O and O–C=O) on Fe/HC-2 and Fe/HC-8 (37.3% and 38.8%) were higher than that on Fe/HC-4 and Fe/HC-6 (34.9% and 35.9%). This might be associated with the higher oxidation ability of Fe^{3+} ions at lower pH (pH 2) and the formation of more iron oxide precipitates at

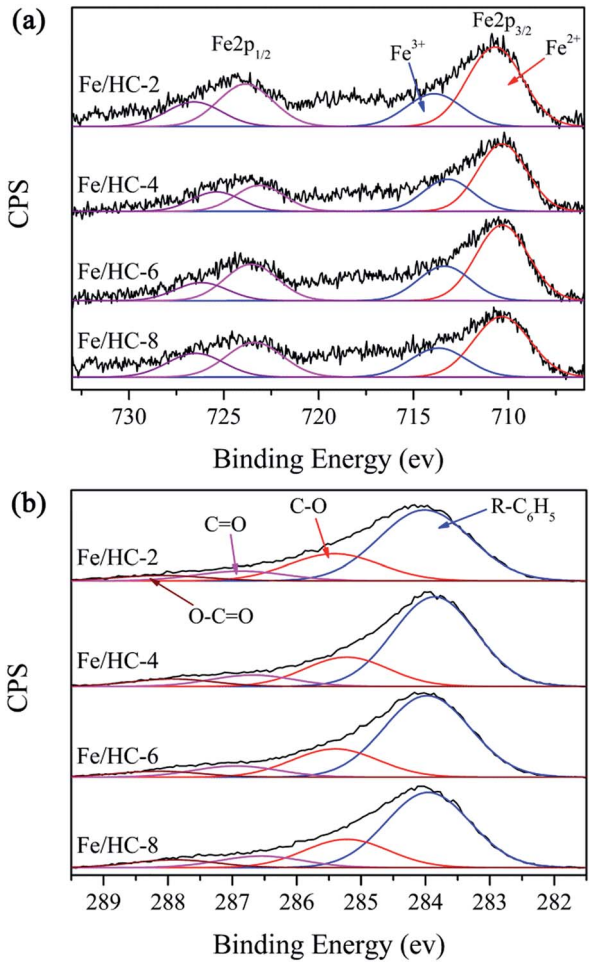

Fig. 5 Fe 2p (a) and C 1s (b) XPS spectra of different Fe/HC samples.

higher pH (pH 8), which might facilitate the dehydration, oxidation and esterification reactions.

Fig. 6 shows the zeta potential of the Fe/HC suspensions at different pH values. No obvious difference was observed for the four samples, and their point of zero charge (PZC) was about 2.1. The sample surface was negatively charged at pHs above pH_{pzc}, and the charge density increased dramatically with increasing pH. Fig. 7 shows the UV-vis diffuse reflectance spectra of different samples. All the samples exhibited excellent light absorption in the visible region, which is beneficial to visible light reactions. Among them, Fe/HC-8 exhibited the strongest absorption.

Photo-Fenton activity of Fe/HC

The dark adsorption results showed that the catalysts exhibited poor adsorption capacity toward Orange II (less than 10%). The reason is that the catalyst surface was highly negatively charged at pH 5, which inhibited the adsorption of anions due to the strong electrostatic repulsion. Among the catalysts, Fe/HC-2 exhibited the lowest adsorption capacity, which can be attributed to its small surface area and pore volume. Fig. 8a shows the Fenton degradation of Orange II over different Fe/HC catalysts. Fe/HC-4 and Fe/HC-6 exhibited poor Fenton activity, and only 25% of Orange II was decolorized at 50 min. Fe/HC-2 and Fe/HC-8 exhibited relatively higher activity, and the decolorization efficiency increased by about 17%. As shown in Fig. 8b, the decolorization of Orange II was significantly enhanced by visible light irradiation. Fe/HC-4 and Fe/HC-6 exhibited similar activity, and Fe/HC-8 showed relatively higher activity. Fe/HC-2 exhibited the highest activity, and more than 90% of Orange II was decolorized. Although Fe/HC-2 had the smallest surface area and pore volume, it exhibited the highest Fenton and photo-Fenton activity. This might be due to its high content of surface Fe^{2+} that can react with H_2O_2 to form $^{\bullet}OH$. Moreover, it had rich oxygen-containing groups, which could change the chemical environment of Fe and might accelerate the regeneration of Fe^{2+} from Fe^{3+}.[44–46] Fig. 9 shows the cycling performance of Fe/HC-2. The decolorization efficiency was still above 90% after seven cycles, demonstrating the good reusability of Fe/HC-2. It is known that the hydrochar is also one kind of organic and may suffer from the degradation under photo-Fenton conditions. On one hand, the hydrochar was produced by a hydrothermal method at 180 °C, suggesting its stable structure in

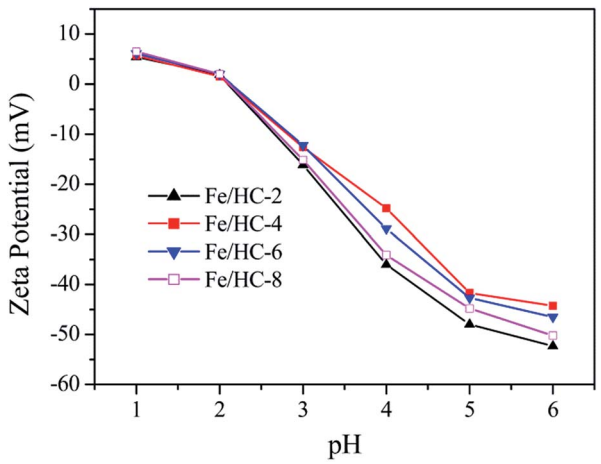

Fig. 6 Zeta potential as a function of pH for different Fe/HC samples.

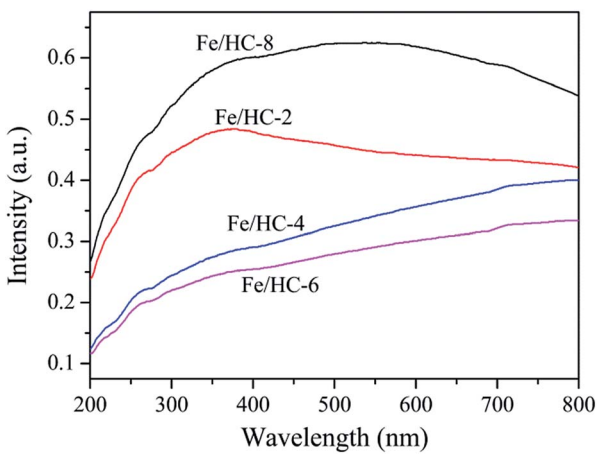

Fig. 7 UV-vis diffuse reflectance spectra of different Fe/HC samples.

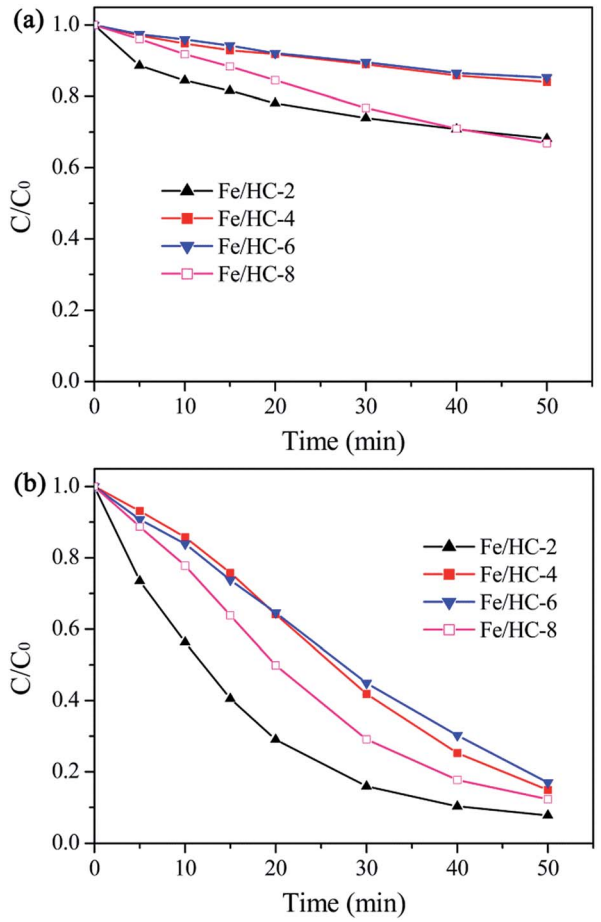

Fig. 8 Decolorization of Orange II in Fenton (a) and photo-Fenton (b) processes with different Fe/HC samples at pH 5.

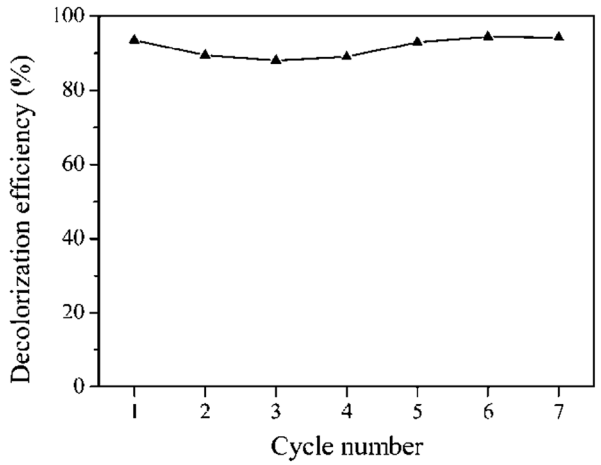

Fig. 9 Decolorization of Orange II for seven successive catalytic experiments with Fe/HC-2.

harsh chemical environment. On the other hand, it had rich oxygen-containing groups on its surface, which are hardly oxidized by the generated radicals. For instance, the ˙OH rate constants of carboxylic acids are far lower than that of Acid Orange.[47,48] Therefore, most of the radicals were consumed by the reaction with Orange II, and the catalyst exhibited a good reusability.

Active species in the Fe/HC photo-Fenton system

It is generally believed that ˙OH can be generated in heterogeneous photo-Fenton process. Fig. 10 shows the formation of ˙OH in different systems using PTA as the probe. The fluorescence intensity increased with reaction time, suggesting the formation of ˙OH. A large amount of ˙OH radicals were produced in different heterogeneous photo-Fenton systems, and the amount of ˙OH generated in the Fe/HC-2 Fenton system was much smaller. The result demonstrated that the visible light irradiation significantly promoted the production of ˙OH. A strong positive correlation was found between the production amount of ˙OH and decolorization efficiency of Orange II, suggesting that ˙OH might played an important role in the heterogeneous Fenton and photo-Fenton reactions. It is well known that ˙OH can be produced through the reaction of Fe^{2+} with H_2O_2, and Fe^{3+} can be reduced to Fe^{2+} by H_2O_2 (eqn (1) and (2)). However, the reduction of Fe^{3+} is extremely slow, resulting in a low oxidation efficiency. Under light irradiation, Fe^{3+} can be reduced in combination with the formation of ˙OH (eqn (3)), thus enhancing the decolorization of Orange II.[49] It can be seen that a small amount of ˙OH radicals were produced in the Fe/HC-2-light system without H_2O_2, demonstrating that ˙OH can be generated through this reaction.

$$H_2O_2 + Fe^{2+} \rightarrow Fe^{3+} + {}^{\cdot}OH + OH^- \quad (1)$$

$$Fe^{3+} + H_2O_2 \rightarrow Fe^{2+} + HO_2^{\cdot} + H^+ \quad (2)$$

$$Fe(OH)^{2+} + h\nu \rightarrow Fe^{2+} + {}^{\cdot}OH \quad (3)$$

Radical trapping experiments were carried out to further clarify the reactive species in this photo-Fenton process. As shown in Fig. 11, both *tert*-butanol (TBA) and iso-propanol (IPA) inhibited the decolorization of Orange II, and IPA had a much

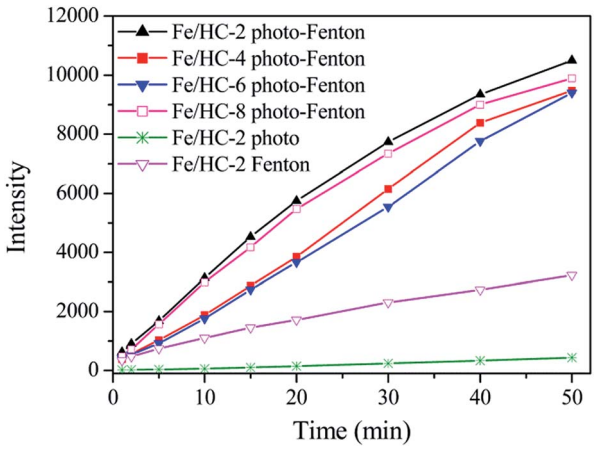

Fig. 10 Formation of hydroxyl radicals in different systems at pH 5.

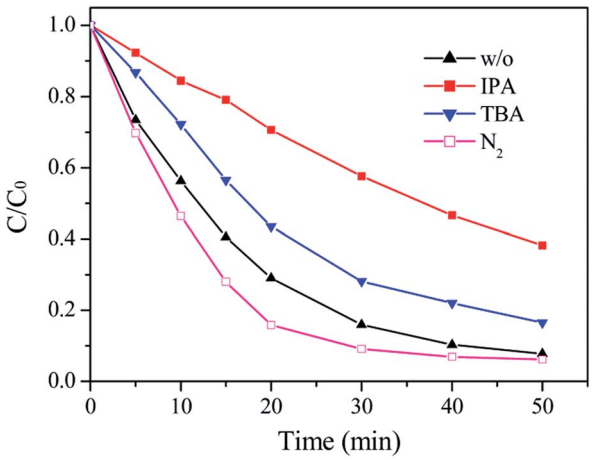

Fig. 11 Effect of scavengers on the photo-Fenton decolorization of Orange II with Fe/HC-2 at pH 5.

stronger inhibitory effect, which can be due to that IPA has a higher rate constant (6×10^9 M^{-1} s^{-1}) with $^{\bullet}OH$ than TBA (6×10^8 M^{-1} s^{-1}).[50] Superoxide radical ($^{\bullet}O_2^-$) is also an active specie in photocatalytic reactions and commonly produced through the reaction between electrons and dissolved O_2. N_2 was bubbled into the catalyst suspension to inhibit the formation of $^{\bullet}O^{2-}$. However, it had little effect on the decolorization of Orange II. In addition, ferrate (VI) ion, another oxidizing specie in Fenton reactions, was not detected. The result further demonstrated that $^{\bullet}OH$ radicals were the main reactive species and the contribution from $^{\bullet}O^{2-}$ and Fe(VI) could be ignored.

Fe leaching in different systems

Since Fe is readily leached during the heterogeneous photo-Fenton process, the contribution from the dissolved Fe cations cannot be ignored. Table 1 shows the change of dissolved Fe with the reaction time in different systems. In the Fe/HC-2 Fenton system, the concentration of total Fe in solution increased very slowly with time, while the leached Fe^{2+} could be ignored, indicating that the decolorization of Orange II without light irradiation was attributed to the heterogeneous reactions. However, the leached total Fe, especially Fe^{2+}, increased significantly under light irradiation. The result indicated that the light irradiation promoted the leaching of Fe and the enhanced activity of the photo-Fenton process compared to the Fenton process was mainly attributed to the dissolved Fe^{2+}. Moreover, the concentrations of the leached Fe^{2+} in different Fe/HC systems were positively correlated with their catalytic efficiencies, further demonstrating that the homogeneous Fenton reaction was responsible for the enhanced decolorization of Orange II. The leached Fe from Fe/HC-2 (0.134 mg L^{-1}) after dark adsorption was much more than that from the other three samples (0.044–0.051 mg L^{-1}), which might be due to the higher surface Fe content of Fe/HC-2. In the Fe/HC-4 and Fe/HC-6 photo-Fenton systems, Fe^{2+} was not detected before 20 min, indicating that the heterogeneous reactions were responsible for the decolorization of Orange II at the initial stage and thereafter the contribution of homogeneous reaction increased significantly. The leached Fe from Fe/HC-2 and Fe/HC-8 during photo-Fenton process was much more than that from Fe/HC-4 and Fe/HC-6, leading to their higher activity. It is worth pointing out that Fe/HC-8 had the lowest surface Fe content. Therefore, the higher leaching of Fe from Fe/HC-8 should be associated its surface groups. Both Fe/HC-2 and Fe/HC-8 had rich oxygen-containing groups, and the loaded Fe might be coordinated to these groups, which could promote the cycle of Fe^{3+}/Fe^{2+}.[6,51,52] The bonds between Fe and oxygen-containing groups could be activated and cleaved with light irradiation.[53,54] Therefore, the photoreduction of Fe^{3+} and Fe leaching occurred simultaneously. Although the surface Fe^{2+}/Fe^{3+} ratio of the catalyst after reaction can be determined by XPS analysis, the leaching of Fe would make the result meaningless.

In order to test this assumption, the changes of Fe^{2+} concentration in the Fe^{2+}-catalyst–H_2O_2 and Fe^{2+}–H_2O_2 photo-Fenton systems were measured, and the amount of H_2O_2 in these experiments was much higher than that of Fe^{2+} in the solution and on the catalyst surface. The concentration of Fe^{2+} decreased significantly due to its reaction with H_2O_2. The

Table 1 Concentration of dissolved total Fe and Fe^{2+} in different systems

		Reaction time (min)			
Reaction system		10	20	30	40
Total Fe (mg L^{-1})	Fe/HC-2/H_2O_2/dye	0.134	0.137	0.161	0.192
	Fe/HC-2/H_2O_2/dye/light	0.479	1.044	1.590	2.194
	Fe/HC-4/H_2O_2/dye/light	0.160	0.398	0.855	1.264
	Fe/HC-6/H_2O_2/dye/light	0.187	0.494	0.852	1.385
	Fe/HC-8/H_2O_2/dye/light	0.233	0.935	1.596	2.455
Fe^{2+} (mg L^{-1})	Fe/HC-2/H_2O_2/dye	0	0	0	0.007
	Fe/HC-2/H_2O_2/dye/light	0.202	0.550	0.942	1.153
	Fe/HC-4/H_2O_2/dye/light	0	0.120	0.516	0.795
	Fe/HC-6/H_2O_2/dye/light	0	0.143	0.418	0.815
	Fe/HC-8/H_2O_2/dye/light	0.168	0.570	0.982	1.388
	Fe^{2+} (10 mg L^{-1})/H_2O_2/light	0.86	0.437	0.311	0.271
	Fe^{2+} (10 mg L^{-1})/H_2O_2/light/Fe/HC-2	1.301	0.86	0.85	0.811
	Fe/HC-2/H_2O_2/light	0.143	0.291	0.487	0.673

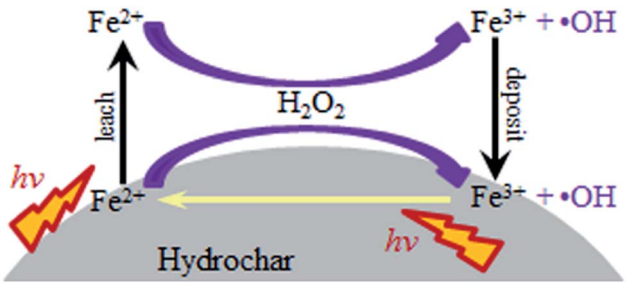

Fig. 12 Proposed mechanism for the Fe^{3+}/Fe^{2+} cycle at the catalyst/water interface.

remained Fe^{2+} in the solution with Fe/HC-2 was much more than that without Fe/HC-2. Since the leached Fe from Fe/HC-2 could not be ignored, its concentration in the catalyst–H_2O_2 system was also determined. It was calculated that the sum of dissolved Fe^{2+} in the catalyst–H_2O_2 and Fe^{2+}–H_2O_2 systems before 40 min were still less than that in the Fe^{2+}-catalyst–H_2O_2 system. The result suggested that HC could promote the reduction of Fe^{3+} to Fe^{2+}.

Possible mechanism for the heterogeneous photo-Fenton reaction

Based on the above results, a possible mechanism for this heterogeneous photo-Fenton process is proposed in Fig. 12. Fe^{2+} on the catalyst surface can react with H_2O_2 to generate $^{\bullet}OH$. Under visible light irradiation, $Fe(OH)^{2+}$ can be reduced to Fe^{2+} in combination with the formation of $^{\bullet}OH$. The light irradiation can promote the leaching of Fe from the catalyst surface. The dissolved Fe^{2+} can also react with H_2O_2 to generate $^{\bullet}OH$ and Fe^{3+}. Fe^{3+} in solution would readily deposit on the catalyst surface at pH 5 due to its low solubility (K_{sp} of $Fe(OH)_3 = 2.79 \times 10^{-39}$). According to literatures, HC with rich oxygen-containing groups could decrease the redox potential of Fe^{3+}/Fe^{2+} and might transfer electrons to Fe^{3+} with light irradiation, thus accelerating the regeneration of Fe^{2+}.[6,49–52] Orange II is oxidized by $^{\bullet}OH$, which can be continuously produced through the Fe^{2+}/Fe^{3+} cycle at the Fe/HC/water interface.

Conclusions

Fe/HC samples were successfully synthesized by a hydrothermal method. It was found the precursor pH affected the structure and property of the samples. Fe/HC-2 had the highest surface Fe content but the smallest surface area and pore volume. The contents of oxygen-containing groups on Fe/HC-2 and Fe/HC-8 were higher than that on Fe/HC-4 and Fe/HC-6. In addition, Fe/HC-8 and Fe/HC-2 exhibited stronger light absorption than Fe/HC-4 and Fe/HC-6. The samples exhibited good photo-Fenton activity for the decolorization of Orange II and their activities followed the order of Fe/HC-2 > Fe/HC-8 > Fe/HC-4 ≈ Fe/HC-6. The higher activities of Fe/HC-2 and Fe/HC-8 were associated with their rich oxygen-containing groups and strong light absorption, which were beneficial to the leaching of Fe and regeneration of Fe^{2+} with light irradiation. Orange II was mainly decolorized by $^{\bullet}OH$ produced from the reaction between H_2O_2 and Fe^{2+} (in solution and on catalyst surface).

Conflicts of interest

There are no conflicts of interest to declare.

Acknowledgements

This work was supported by the National Natural Science Foundation of China (No. 21207032), and the Natural Science Foundation of Hebei Education Department (No. ZD2017042).

Notes and references

1 K. E. O'Shea, *J. Phys. Chem. Lett.*, 2012, **3**, 2112.
2 P. V. Nidheesh, *RSC Adv.*, 2015, **5**, 40552.
3 A. Cihanoğlu, G. Gündüz and M. Dükkancı, *Appl. Catal., B*, 2015, **165**, 687.
4 L. Zhou, J. Ma, H. Zhang, Y. Shao and Y. Li, *Appl. Surf. Sci.*, 2015, **324**, 490.
5 J. Shi, Z. Ai and L. Zhang, *Water Res.*, 2014, **59**, 145.
6 Z. Ma, L. Ren, S. Xing, Y. Wu and Y. Gao, *J. Phys. Chem. C*, 2015, **119**, 23068.
7 S. Xing, D. Zhao, W. Yang, Z. Ma, Y. Wu, Y. Gao and W. Chen, *J. Mater. Chem. A*, 2013, **1**, 1694.
8 F. Martínez, R. Molina, M. I. Pariente, J. A. Siles and J. A. Melero, *Catal. Today*, 2017, **280**, 176.
9 D. Wan, W. Li, G. Wang, L. Lu and X. Wei, *Sci. Total Environ.*, 2017, **574**, 1326.
10 N. Banić, B. Abramović, J. Krstić, D. Šojić, D. Lončarević, Z. Cherkezova-Zheleva and V. Guzsvány, *Appl. Catal., B*, 2011, **107**, 363.
11 G. M. S. ElShafei, F. Z. Yehia, G. Eshaq and A. E. ElMetwally, *Sep. Purif. Technol.*, 2017, **178**, 122.
12 A. Babuponnusamia and K. Muthukumar, *Chem. Eng. J.*, 2012, **183**, 1.
13 Y. Ahmed, Z. Yaakob and P. Akhtar, *Catal. Sci. Technol.*, 2016, **6**, 1222.
14 Y. Ju, Y. Yu, X. Wang, M. Xiang, L. Li, D. Deng and D. D. Dionysiou, *J. Hazard. Mater.*, 2017, **323**, 611.
15 A. N. Soon and B. H. Hameed, *Appl. Catal., A*, 2013, **450**, 96.
16 Y. Gao, Y. Wang and H. Zhang, *Appl. Catal., B*, 2015, **178**, 29.
17 Q. Chen, P. Wu, Y. Li, N. Zhu and Z. Dang, *J. Hazard. Mater.*, 2009, **168**, 901.
18 H. Wang, Y. Xu, L. Jing, S. Huang, Y. Zhao, M. He, H. Xu and H. Li, *J. Alloys Compd.*, 2017, **710**, 510.
19 T. Soltani and B. K. Lee, *J. Mol. Catal. A: Chem.*, 2016, **425**, 199.
20 H. Zeng, X. Liu, T. Wei, X. Li, T. Liu, X. Min, Q. Zhu, X. Zhao and J. Li, *RSC Adv.*, 2017, **7**, 23787.
21 T. Soltani and B. K. Lee, *Chem. Eng. J.*, 2017, **313**, 1258.
22 C. Chen, Y. Zhou, N. Wang, L. Cheng and H. Ding, *RSC Adv.*, 2015, **5**, 95523.
23 C. Cai, Z. Zhang, J. Liu, N. Shan, H. Zhang and D. D. Dionysiou, *Appl. Catal., B*, 2016, **182**, 456.

24 Y. Wang, M. Liang, J. Fang, J. Fu and X. Chen, *Chemosphere*, 2017, **182**, 468.
25 J. R. Kim and E. Kan, *J. Ind. Eng. Chem.*, 2015, **21**, 644.
26 Y. Zhou, B. Xiao, S. Q. Liu, Z. Meng, Z. G. Chen, C. Y. Zou, C. B. Liu, F. Chen and X. Zhou, *Chem. Eng. J.*, 2016, **283**, 266.
27 Y. Yao, J. Qin, Y. Cai, F. Wei, F. Lu and S. Wang, *Environ. Sci. Pollut. Res.*, 2014, **21**, 7296.
28 B. Hu, K. Wang, L. Wu, S. H. Yu, M. Antonietti and M. M. Titirici, *Adv. Mater.*, 2010, **22**, 813.
29 Y. Wang, Z. Ao, H. Sun, X. Duan and S. Wang, *Appl. Catal., B*, 2016, **198**, 295.
30 G. Zhou, L. Zhou, H. Sun, H. M. Ang, M. O. Tadé and S. Wang, *Chem. Eng. Res. Des.*, 2015, **101**, 15.
31 Z. Luo, L. Qu, T. Han, Z. Zhang, X. Shao, X. Wu and Z. Chen, *Eur. J. Inorg. Chem.*, 2014, **2014**, 994.
32 X. Zuo, M. Chen, D. Fu and H. Li, *Chem. Eng. J.*, 2016, **294**, 202.
33 Z. Luo, H. Tang, L. Qu, T. Han and X. Wu, *CrystEngComm*, 2012, **14**, 5710.
34 H. Sun, G. Zhou, S. Liu, H. M. Ang, M. O. Tadé and S. Wang, *ACS Appl. Mater. Interfaces*, 2012, **4**, 6235.
35 Y. Wang, H. Sun, X. Duan, H. M. Ang, M. O. Tadé and S. Wang, *Appl. Catal., B*, 2015, **172–173**, 73.
36 M. Saran and K. H. Summer, *Free Radical Res.*, 1999, **31**, 429.
37 S. M. Kang, X. L. Li, J. Fan and J. Chang, *Ind. Eng. Chem. Res.*, 2012, **51**, 9023.
38 X. Y. Chen, C. Chen, Z. J. Zhang, D. H. Xie and J. W. Liu, *J. Colloid Interface Sci.*, 2013, **398**, 176.
39 R. Demir-Cakan, N. Baccile, M. Antonietti and M. M. Titirici, *Chem. Mater.*, 2009, **21**, 484.
40 M. Li, W. Li and S. Liu, *Carbohydr. Res.*, 2011, **346**, 999.
41 H. S. Qian, S. H. Yu, L. B. Luo, J. Y. Gong, L. F. Fei and X. M. Liu, *Chem. Mater.*, 2006, **18**, 2102.
42 H. Lin, H. Zhang and L. W. Hou, *J. Hazard. Mater.*, 2014, **276**, 182.
43 M. Sevilla and A. B. Fuertes, *Carbon*, 2009, **47**, 2281.
44 G. Fang, J. Gao, C. Liu, D. D. Dionysiou, Y. Wang and D. Zhou, *Environ. Sci. Technol.*, 2014, **48**, 1902.
45 T. J. Strathmann and A. T. Stone, *Environ. Sci. Technol.*, 2002, **36**, 5172.
46 Z. Ma, X. Wei, S. Xing and J. Li, *Catal. Commun.*, 2015, **67**, 68.
47 S. Hammami, N. Bellakhal, N. Oturan, M. A. Oturan and M. Dachraoui, *Chemosphere*, 2008, **73**, 678.
48 S. Xing, X. Lu, L. Ren and Z. Ma, *RSC Adv.*, 2015, **5**, 60279.
49 J. Herney-Ramirez, M. A. Vicente and L. M. Madeira, *Appl. Catal., B*, 2010, **98**, 10.
50 G. V. Buxton, C. Greenstock, W. P. Hellman and A. B. Ross, *J. Phys. Chem. Ref. Data*, 1988, **17**, 513.
51 N. Wang, L. Zhu, M. Lei, Y. She, M. Cao and H. Tang, *ACS Catal.*, 2011, **1**, 1193.
52 Y. Qin, L. Zhang and T. An, *ACS Appl. Mater. Interfaces*, 2017, **9**, 17115.
53 M. I. Polo-López, I. García-Fernández, T. Velegraki, A. Katsoni, I. Oller, D. Mantzavinos and P. Fernández-Ibáñez, *Appl. Catal., B*, 2012, **111–112**, 545.
54 M. J. Hernández-Rodríguez, C. Fernández-Rodríguez, J. M. Doña-Rodríguez, O. M. González-Díaz, D. Zerbani and J. Pérez Peña, *J. Environ. Chem. Eng.*, 2014, **2**, 163.